1661-8726/08/010085–14
DOI 10.1007/s00015-007-1245-x
Birkhäuser Verlag, Basel, 2008

Swiss J. Geosci. 101 (2008) 85–98

The Mount Cameroon 1959 compound lava flow field: morphology, petrography and geochemistry

Manga S. Njome*,[1], Cheo E. Suh[1], R. Stephen J. Sparks[2], Samuel N. Ayonghe[1] & J. Godfrey Fitton[3]

Key words: Mt. Cameroon, 1959 compound flow field, aa lava, basanite/hawaiite.

ABSTRACT

The Mount Cameroon 1959 compound lava flow field (volume ~3.4×10^7 m^3; mean effusion rate ~13 m^3 s^{-1}–18 m^3 s^{-1}) is the only twentieth century eruption not following the NE–SW fracture system, the pathway for other recorded eruptions. The eruption occurred at two sites: 2006 m–1961 m and 1500 m, typically an aa flow with small pahoehoe channels in proximal regions. Morphologically, lava tubes and inflation hollows characterize upper flow regions while compression ridges and lava pinnacles characterize distal regions. Evidence of lava flow stagnation with time is provided by distinct layers at channel walls in proximal zones. Such channels are very narrow, deep, with poorly developed levee structures, attesting to high effusion rate and initial rapid advance of lava. The 1959 basanites show geochemical signatures and textural features indicating early fractionation of olivine and diopside, followed by Fe-Ti oxides and plagioclase. More evolved 1961 m vents lavas show higher incompatible and lower compatible element contents than those from the 1500 m sites. We interpret this to mean that residual more evolved magma of the 1954 eruption was initially forced out by degassing of a new less evolved magma batch, which finally drained out at the lower 1500 m site, the two magma batches not mixing. Incompatible elements indicate that the 1959 lava is similar to other historic lavas. However, subtle differences in compatible and incompatible element ratios (e.g. V/Rb) suggest that magma is erupted from the volcano in discrete batches from different magma storage regions rather than from a single large evolving chamber. The low whole-rock Mg contents (5.5 wt% MgO, average Mg# = 33.9) and high differentiation index values (36.7–38.5) for the 1959 lavas show that they are the most fractionated of all twentieth century Mt. Cameroon lavas.

Introduction

Mount Cameroon (04° 13' N, 09° 10' E) is located in Southwestern Cameroon and rises from the coast to a height of 4095 m a.s.l. (Fig. 1), making it the highest mountain in equatorial Africa and third in Africa, after Kilimanjaro (5963 m) and Mount Kenya (5194 m). It covers a total area of ~1116 km^2. It is extensively covered by cinder cones, explosive craters, lava flows and scoraceous lapilli. Mount Cameroon is part of the NE–SW alignment of Tertiary to Recent volcanic and sub-volcanic complexes located in both central Africa and the adjacent South Atlantic ocean (Moreau et al. 1987), known as the Cameroon Volcanic Line (CVL). The CVL is described in Geze (1953); Fitton (1980, 1987); Moreau et al. (1987); Halliday et al. (1990); Ballentine et al. (1997); Ubangoh et al. (1998); Marzoli et al. (2000); Suh et al. (2003); Njome et al. (2003) and references therein. Mount Cameroon remains the only active volcano of the CVL, having erupted seven times in the last century (Fig. 1). Although Mount Cameroon is a major regional source of hazard, it remains one of the least studied of active volcanoes around the world. Most studies of the CVL have focused on the regional–scale petrological aspects of the line rather than on specific volcanological investigations (Fitton, 1980; Fitton & Dunlop 1985; Moreau et al. 1987; Halliday et al. 1988, 1990; Ubangoh et al. 1998; Marzoli et al. 1999, 2000; Rankenburg et al. 2004).

Monitoring, hazard assessment and disaster mitigation at Mount Cameroon call for a better understanding of the volcano's eruptive behaviour. This requires a study of the lava flow morphology since this provides indications of effusion rates and flow rates necessary for planning evacuations, for example, in subsequent eruptions. Also, the petrochemical characteristics of eruptive products provide insights into the magma storage and plumbing system and these data are relevant in designing more appropriate monitoring techniques. This study concerns the 1959 lava flow field. The 1982, 1999 and 2000 eruptions have

[1] Department of Geology and Environmental Science, University of Buea, P.O. Box 63, Buea, South West Province, Cameroon.
E-mails: MSN: mnjome@yahoo.com; CES: chuhma@yahoo.com; SNA: samayonghe@yahoo.com
[2] Department of Earth Sciences, University of Bristol, Wills Memorial Building, Queens Road, Bristol, BS8 1RJ, U.K. E-mail: steve.sparks@bristol.ac.uk
[3] School of GeoSciences, University of Edinburgh, Grant Institute, West Mains Road, Edinburgh, EH9 3JW, U.K.
E-mail: godfrey.fitton@ed.ac.uk
*Corresponding author: M.S. Njome. E-mail: mnjome@yahoo.com

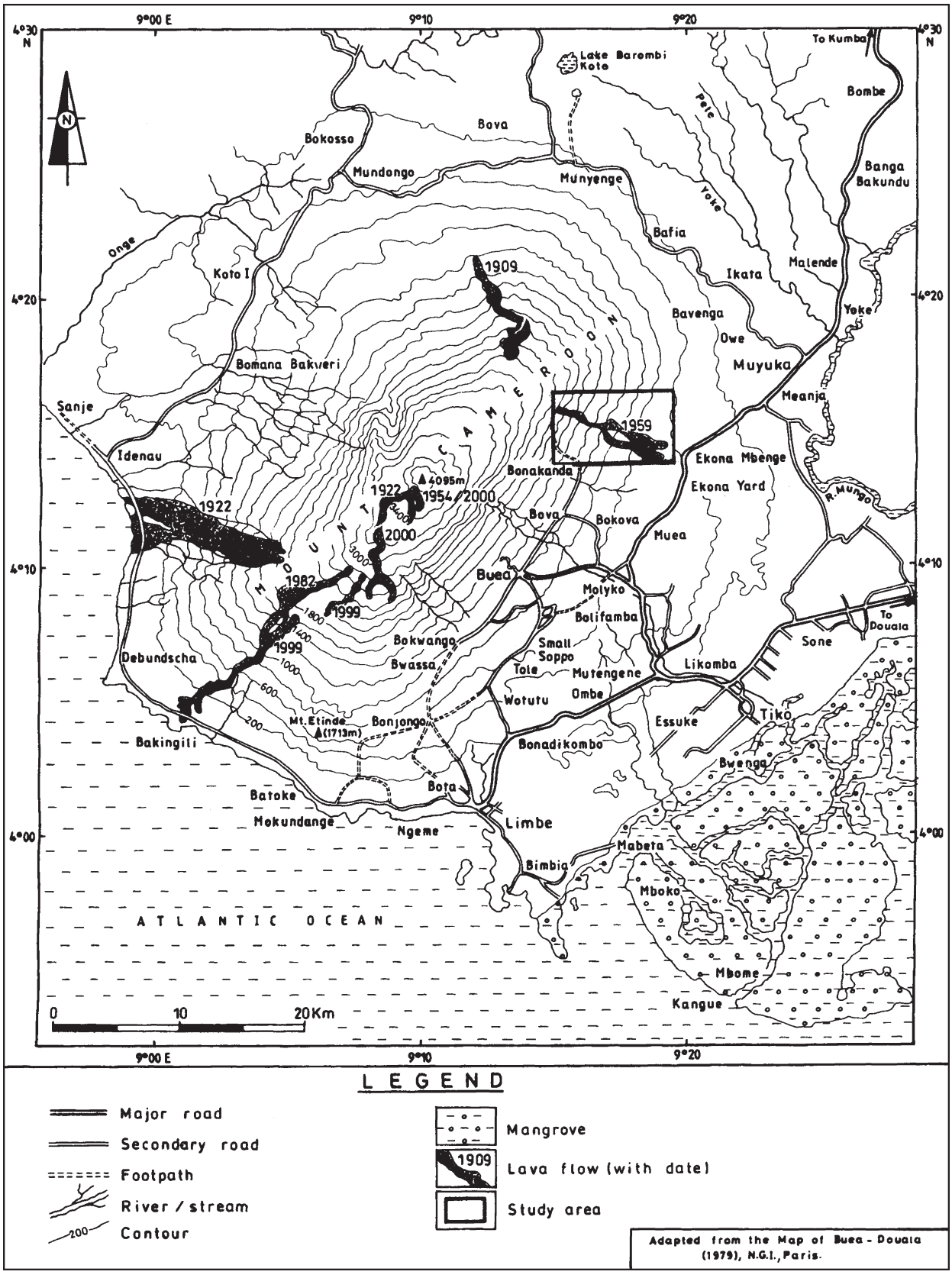

Fig. 1. Contour map of Mount Cameroon showing the 20th century lava flows. Year of eruption indicated, with the 1959 flow enclosed in a rectangular box.

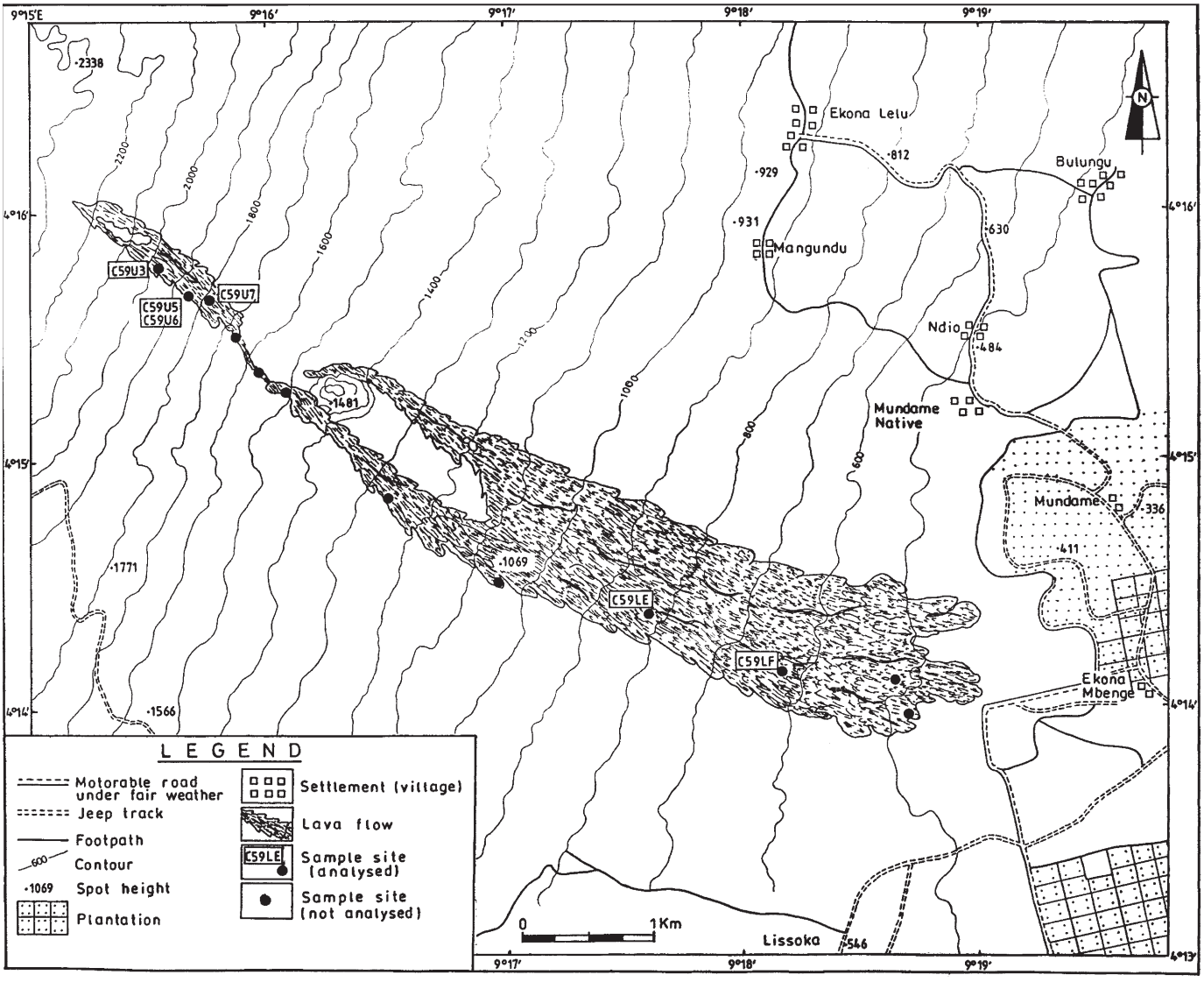

Fig. 2. Map of the entire 1959 Mount Cameroon lava flow field produced by the February–March eruption. Sample sites indicated.

received greater attention (Fitton et al. 1983; Deruelle et al. 2000; and Suh et al. 2003).

The 1959 eruption sites and flow morphology

The February to March 1959 eruption (Jennings 1959) threatened the town of Ekona (Fig. 2), stopping 1 km from the town and destroying small farm lands. The distribution of eruption sites around Mt. Cameroon (Fig. 1) demark a NE–SW fracture system (inherited from the shear zone within the underlying basement) that must have acted as the pathway for magma. However, the 1959 lava was emitted on the north-eastern flank from a NW–SE fissure (Fig. 1). In the 1959 flow field (04° 14' 40" N, 09°17' 30" E; Fig. 2), the flow extends approximately NW–SE (WNW–ESE). The flow originated from a height of 1961 m a.s.l. extending to a distance of ~7.75 km (Fig. 2). The lava formed two main branches and it is widest (1900 m) where these coalesce. The flow field covers a total area of ~4.5×10^6 m^2. Flow thickness varies from ~12 m at the front to ~5 m in shallow medial channels. This gives an estimated lava volume of ~2.3×10^7 m^3–~5.4×10^7 m^3 (with a mean of ~3.4×10^7 m^3). The eruption lasted 22–30 days in February and March (Jennings 1959) and we estimate a mean effusion rate of 13 m^3 s^{-1}–18 m^3 s^{-1}.

The 1959 lava morphology varies according to proximity to the vents, underlying topography and local flow evolution. There are two major explosive vents (cinder cones) and about 5 smaller vents (spatter cones) oriented WNW–ESE. The earliest vent (at 1961 m) is an elliptical crater elongated in the NW–SE direction and dissected by the fissure that runs through it. At

higher elevations there are smaller craters, which formed before a major explosive vent (at 1976 m), a cinder cone, smaller than the 1961 m cone. Northwest of this cone at higher elevations are two late vents. A small hornito (at 1994 m, Fig. 3a) formed after the 1976 m vent about 10 m away from the last vent that opened (at 2006 m a.s.l.), a small bocca with the last drain of pahoehoe lava.

Channels in the 1959 lava flow field widen away from the vents. This can be accounted for by the numerous lava tubes sourced from the main vent, forming an interconnecting network of underground channels through which lava drains out, thus effectively widening the flow field. The number of lava tubes decreases away from the vents with the last major tube observed at a distance of about 4.75 km from the vent. Inflation and collapse structures are observed within the first 2 km of the flow and mark regions where lava within flow tubes become stuck and pressurized for some time before draining out. The structures are elliptical and elongated in the same WNW–ESE direction as the flow.

The flows comprise single or multiple channels, bounded by well-defined levees. Most commonly, the channels at the upper site flows are quite narrow and deep with less well-developed levee structures commonly showing distinct horizontal layers (each layer being ~10–15 cm thick). Channel widths vary greatly (60 cm–132 m). Proximal pahoehoe channels effusing from boccas and tubes are usually <1 m wide (Fig. 3b), while distal blocky-aa channels, range between 10 m to over 100 m in width. Thermally mature aa is typically composed of a variety of clasts, abraded clinker, fractured angular blocks of massive lava and fragments of welded breccias (Fig. 3c).

Following the work of Sparks et al. (1976), two main types of levees were identified: initial levees and rubble levees. Occasionally drained channels show massive lava on the inside walls of levees underlying areas of welded breccias, clinker or overflow drapes (Fig. 3c, left wall). Such plastic aa bulwarks represent initial levees. Rubble levees, the most common levee type observed, is composed of highly brecciated clinker, blocks and rubble of varying sizes, which can be loosely packed or commonly welded (Fig. 3c, right wall and top of levees). Typically, the levees display two distinct parts: outer relatively gentle slopes (typical slope angle of ~35°) and steeper inner walls (typical slope angle of ~50°).

Morphological features which form commonly towards the flow front include pressure ridges and lava pinnacles. Pressure ridges are wave-like surfaces of lavas across the main flow direction. Their predominance towards the lava front can be interpreted as due to compression through flow-front stiffening and stagnation as increasingly cooled magma reaches the flow front as the lava advances. Average measured wavelength (crest to crest distance) for the ridges is 13.62 m while the average ridge width is 4.6 m. The ridges have an average height of 2.2 m. The wavelengths of ridges decrease towards the flow front with typical values of >20 m where the ridges begin to <11 m close to the front. Lava pinnacles (projection of slabs of lava or rafts of welded breccias thrust out of blocky channels are more abundant at the lava flow front, where cooling has resulted to increased viscosity of the lava. The pinnacles are typically composed of brecciated material (Fig. 3d).

At a distance of about 1.6 km from the main vents at 1500 m a.s.l., no specific vent could be identified due to the thick forest cover. However, the predominance of deep-narrow chan-

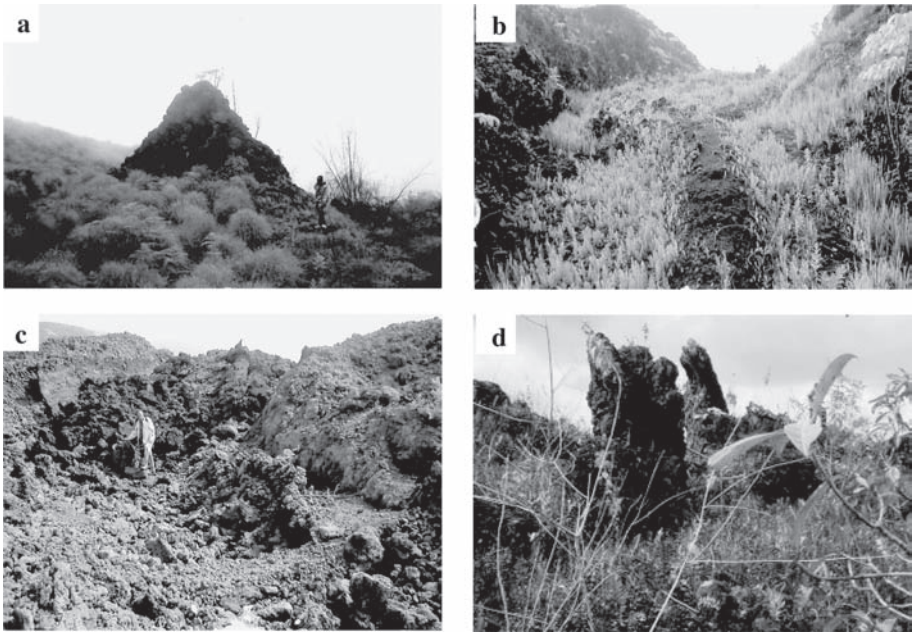

Fig. 3. Morphological features of the 1959 lava flow field. a) The most extreme vent of the upper site Mt. Cameroon 1959 eruption – a spatter cone forming a small hornito. b) A narrow proximal pahoehoe flow issuing out at the centre of the main vent, forming the central part of a lava channel which is made up of aa lava at its wider margins. c) Thermally mature aa of the 1959 Mt. Cameroon flow field. The figure stands at the centre of the channel, made up of fractured angular blocks of massive lava. Note the initial levee at the left wall, overlaid by loose rubble, same material which characterizes the rubble levee of the right wall. d) Projection of slabs of lava and rafts of welded breccias as lava pinnacles – typical feature which characterizes the flow front.

Table 1. Modal composition of representative 1959 Mt. Cameroon lava samples (vol%) determined by counting 2000 points. SiO_2 (wt%) shown for comparison.

Sample No.	Location (Lat. & Long.)	Elevation	SiO_2	Olivine	Pyroxene	Plagioclase	Iron Oxides	Groundmass	Vesicle	Phenocryst content
C59U3	04° 15' 45" N 09° 15' 32" E	1911 m	46.43	1.7	7.8	3.2	0.6	58.0	28.6	13.3
C59U5	04° 15' 40" N 09° 15' 37" E	1824 m	46.27	0.5	7.9	3.9	0.6	68.0	18.9	12.9
C59U7	04° 15' 40" N 09° 15' 44" E	1762 m	46.20	0.0	10.8	2.6	1.8	74.2	10.4	15.2
C59LE	04° 14' 22" N 09° 17' 34" E	777 m	45.95	0.3	6.5	3.2	0.6	82.2	6.8	10.6
C59LF	04° 14' 09" N 09° 18' 10" E	581 m	46.21	1.1	8.5	3.4	0.9	82.4	3.5	13.9

nels, pahoehoe drains, inflation structures and widening of the flow away from this area (Fig. 2), indicates outburst of lava at a lower site. We infer that, like the 1922, 1999 and 2000 eruptions, the 1959 eruption was active at two sites, with the upper site vents being more explosive (producing cinder cones) while the lower sites produced degassed magma. Previous workers stated that the eruption occurred at a height of 1500 m (Ubangoh et al. 1997; Suh et al. 2003).

Textures and mineralogy

Eleven representative samples were systematically collected from the vent to the front (Fig. 2). The bulk chemistry of six samples was analyzed. Petrographically, the samples are quite similar and are porphyritic. Point-counted modal analyses for representative samples (Table 1) show that phenocryst contents vary from 10.6–15.2 vol% and vesicle abundance varies from 3.5–28.6 vol% with a general decrease from the vents to the front. They contain olivine, clinopyroxene, plagioclase and Fe-Ti oxides, both as phenocrysts (size >0.3 mm) and as groundmass microlites.

Clinopyroxene is the dominant phenocryst phase (6.5–10.8 vol%, Table 1) with a crystal range between 0.6–2.75 mm. The clinopyroxenes show two distinct types. Most commonly they occur as crystal aggregates either on their own, or together with plagioclases and/or Fe-Ti oxides, and rarely with olivine, giving the rocks a glomeroporphyritic texture (Fig. 4a). The second type occurs as single individual large euhedral–subhedral crystals sometimes with enclosed or partially enclosed laths of plagioclases (Fig. 4b). Some crystals show resorption either at the margins, centre or growth zone boundaries (Fig. 4b). A few clinopyroxene crystals display fractures filled by groundmass.

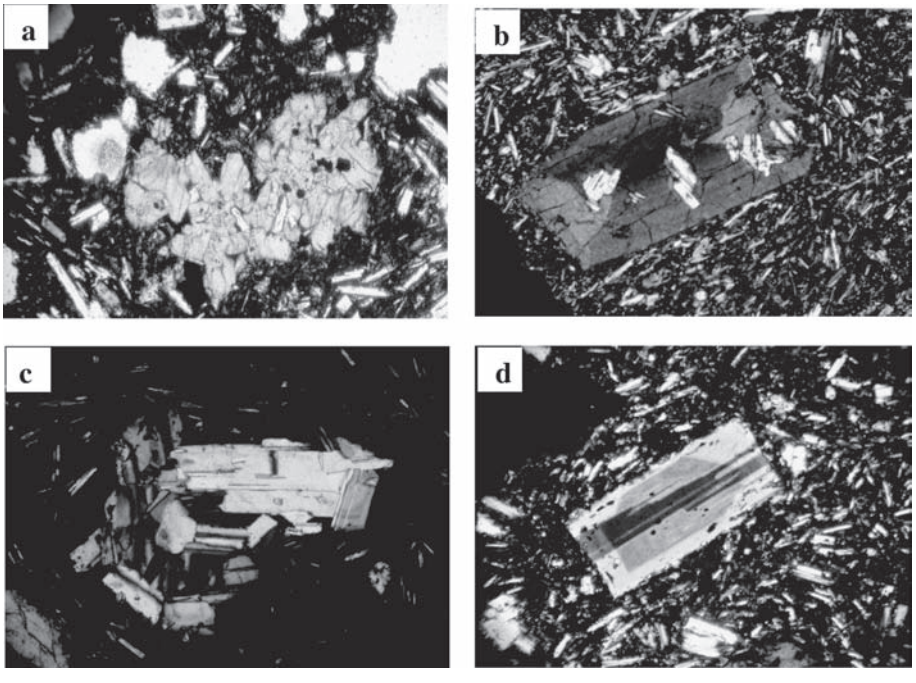

Fig. 4. Photomicrographs of representative 1959 Mt. Cameroon basalts. a) Glomeroporphyritic texture showing aggregate crystals of titanomagnetite (opaque), plagioclase (white) and clinopyroxene (brownish-green). The aggregate length is 0.6 mm. b) Isolated resorbed, twinned and zoned clinopyroxene crystal (pale-green) enclosing laths of plagioclase (white), giving a typical ophitic texture (crystal is 0.8 mm long). c) Aggregate of plagioclase sub-grains (whitish) occurring in exclusive clot (clot length is 1.0 mm). d) Large plagioclase phenocryst (largest crystal) with slightly resorbed margins, well zoned and twinned (crystal is 0.6 mm long).

Table 2. Representative electron microprobe analyses of olivine.

Sample C59LE (Lower site)										
Analysis No.	1	2	3	4	5	6	7	8	9	10
Region	**m**	**m**	**r**	**r**	**c**	**c**	**c**	**c**	**c**	**c**
SiO_2	37.55	35.95	38.86	37.16	38.53	37.80	37.56	38.05	38.13	37.48
TiO_2	0.10	0.07	0.07	0.08	0.04	0.02	0.03	0.02	0.01	0.00
Al_2O_3	0.02	0.05	0.00	0.00	0.00	0.00	0.01	0.01	0.00	0.00
Cr_2O_3	0.01	0.00	0.01	0.00	0.00	0.01	0.00	0.03	0.01	0.00
FeO	23.01	26.63	20.04	24.09	18.09	20.17	20.79	19.55	17.92	20.69
NiO	0.07	0.05	0.12	0.04	0.13	0.12	0.04	0.13	0.12	0.05
MnO	0.46	0.67	0.37	0.51	0.30	0.39	0.37	0.39	0.26	0.41
MgO	37.93	33.49	40.47	36.41	41.77	40.12	39.62	40.12	41.56	39.63
CaO	0.35	0.41	0.34	0.35	0.30	0.29	0.27	0.29	0.30	0.28
Na_2O	0.00	0.04	0.03	0.00	0.00	0.00	0.02	0.00	0.00	0.01
Total	99.49	97.35	100.3	98.64	99.16	98.92	98.72	98.60	98.31	98.56
Si^{4+}	0.99	0.99	1.00	0.99	0.99	0.99	0.99	0.99	0.99	0.99
Fe^{2+}	0.51	0.61	0.43	0.54	0.39	0.44	0.46	0.43	0.39	0.46
Mn^{2+}	0.01	0.01	0.01	0.01	0.01	0.01	0.01	0.01	0.01	0.01
Mg^{2+}	1.49	1.37	1.55	1.45	1.60	1.56	1.55	1.56	1.61	1.55
Ca^{2+}	0.01	0.01	0.01	0.01	0.01	0.01	0.01	0.01	0.01	0.01
Total	3.01	2.99	3.00	3.00	3.00	3.01	3.02	3.00	3.01	3.02
Fo%	74.6	69.2	78.3	72.9	80.5	78.0	77.3	78.5	80.5	77.4
Fa%	25.4	30.9	21.7	27.1	19.6	22.0	22.7	21.5	19.5	22.7

Structural formulae calculated on the basis of four oxygen anions and total iron expressed as Fe^{2+}. r: rim; c: core (of phenocryst); m: microlite; Fo: forsterite; Fa: fayalite. $Fo\% = 100Mg^{2+}/(Mg^{2+} + Fe^{2+})$; $Fa\% = 100Fe^{2+}/(Fe^{2+} + Mg^{2+})$.

Plagioclase is the next dominant phenocryst phase (2.6–3.9 vol%; Table 1), occurring with typical size range of 0.5–1.6 mm. Three different plagioclase types are recognized: as aggregates of sub-grains {usually smaller (0.1–0.5 mm) and anhedral in form: microphenocrysts} in monomineralic clots or polymict aggregates with mostly clinopyroxene and/or Fe-Ti oxides (Fig. 4c); as single slightly resorbed large (0.5–1.6 mm) phenocrysts, subhedral to euhedral in outline and typically zoned (Fig. 4d) and as laths, forming the groundmass microlites (<0.1 mm).

Olivine typically occurs as isolated, large (0.5–2.4 mm), optically unzoned crystals in most samples and is the least abundant phenocryst phase of the silicates (0.0–1.7 vol%; Table 1). Inclusions are generally rare and mostly Fe-Ti oxides with a few tiny melt inclusions.

The Fe-Ti oxides occur as individual microphenocrysts, as aggregates with clinopyroxene and plagioclase (Fig. 4a) and as inclusions in clinopyroxene. A few occur as large phenocrysts (0.6–1.8 mm; Table 1).

The groundmass is generally microlite-rich (>75 vol%) most of which are plagioclase with some minor amounts of clinopyroxene, olivine and Fe-Ti oxides set within a dark-brown glass. Groundmass texture is commonly trachytic.

Mineral chemistry

Mineral analyses were obtained on a JEOL JXA 8600 SUPERPROBE electron microprobe at the University of Bristol. The operating parameters were 20 nA beam current and 20 kV accelerating voltage, with a beam size of 1 μm.

Representative microprobe analyses of olivine phenocrysts are given in Table 2. The crystals are slightly normally zoned with the cores being richer in magnesium ($Fo_{77–81}$) than the rims (Fo_{73}-Fo_{78}). The intra-grain range in forsterite content is narrow (2–4%). The Fe-rich character of the olivines reflects the evolved nature of the magma. Microlites are more iron-rich ($Fo_{69–75}$) than the phenocrysts ($Fo_{81–77}$), and overlap in composition with phenocryst rims.

Representative microprobe analyses of clinopyroxene are presented in Table 3. The overall clinopyroxene mean composition is $Wo_{47–50}\,En_{36–41}\,Fs_{10–14}$ (with a range from $Wo_{47.3}\,En_{39.4}\,Fs_{13}$ to $Wo_{49.8}\,En_{36.3}\,Fs_{13.7}$) and classifies as diopside on the En-Wo-Fs ternary nomenclature plot (after Morimoto 1989). The Mg#, $100Mg^{2+}/(Mg^{2+} + Fe^{2+})$, ranges from 74 to 81 with the cores of phenocrysts being less evolved (Mg# = 77–81) than the rims (Mg# = 74–78). The Mg# for the microlites and microphenocrysts fall within the same range as those at the rim of phenocrysts. Aluminium is partitioned between tetrahedral and octahedral sites in ratios generally between 4.2:1 and 8.5:1. The two clinopyroxene populations identified under the microscope also differ slightly in composition from the isolated phenocrysts having a lower TiO_2 and higher Mg# (<6 wt% and 77–81 respectively) compared to the aggregate phenocrysts that have a higher TiO_2 and lower Mg# (>6 wt% and 76–79 respectively). Also, the isolated phenocrysts have higher SiO_2, MgO and CaO than the aggregate phenocrysts.

Table 3: Representative electron microprobe analyses of clinopyroxene.

Sample C59LE (lower site)										
Analysis No.	1	2	3	4	5	6	7	8	9	10
Region	**m**	**mph**	**r**	**r**	**r**	**r**	**c**	**c**	**c**	**c**
SiO_2	48.37	46.49	44.31	48.04	46.29	48.68	48.11	47.65	48.57	47.12
TiO_2	2.33	2.64	3.75	2.16	2.42	2.30	1.81	2.07	1.60	2.45
Al_2O_3	4.22	6.05	8.16	5.96	6.39	4.20	5.29	5.95	5.09	6.07
Cr_2O_3	0.03	0.01	0.02	0.07	0.02	0.00	0.00	0.20	0.13	0.03
FeO	7.87	7.09	8.01	6.78	7.00	7.71	7.29	6.44	6.98	7.03
NiO	0.00	0.03	0.01	0.04	0.00	0.02	0.00	0.04	0.03	0.01
MnO	0.19	0.14	0.15	0.10	0.10	0.19	0.12	0.10	0.15	0.20
MgO	13.38	13.14	11.89	13.72	13.06	13.46	13.76	13.95	13.98	13.32
CaO	22.40	22.81	22.70	23.08	23.31	22.46	22.65	23.05	23.08	22.83
Na_2O	0.60	0.60	0.58	0.42	0.52	0.45	0.54	0.52	0.43	0.61
K_2O	0.00	0.00	0.00	0.00	0.00	0.00	0.00	0.00	0.00	0.00
Total	99.39	99.00	99.57	100.36	99.12	99.48	99.57	99.99	100.05	99.66
Mg#	76.63	78.22	74.22	79.77	78.44	77.10	78.60	80.82	79.47	78.44
Si^{4+}	1.83	1.76	1.68	1.79	1.75	1.83	1.81	1.78	1.81	1.77
Ti^{4+}	0.07	0.08	0.11	0.06	0.07	0.07	0.05	0.06	0.04	0.07
Al^{3+}	0.19	0.27	0.36	0.26	0.29	0.19	0.23	0.26	0.22	0.27
Cr^{3+}	0.00	0.00	0.00	0.00	0.00	0.00	0.00	0.01	0.00	0.00
Fe^{2+}	0.25	0.22	0.25	0.21	0.22	0.24	0.23	0.20	0.22	0.22
Ni^{2+}	0.00	0.00	0.00	0.00	0.00	0.00	0.00	0.00	0.00	0.00
Mn^{2+}	0.00	0.00	0.00	0.00	0.00	0.01	0.00	0.00	0.00	0.01
Mg^{2+}	0.75	0.74	0.67	0.76	0.74	0.76	0.77	0.78	0.78	0.75
Ca^{2+}	0.91	0.93	0.92	0.92	0.95	0.91	0.91	0.92	0.92	0.92
Na^{+}	0.04	0.04	0.04	0.03	0.04	0.03	0.04	0.04	0.03	0.04
Al^{iv}	0.17	0.24	0.32	0.21	0.25	0.17	0.19	0.22	0.19	0.23
Al^{vi}	0.02	0.03	0.04	0.05	0.04	0.02	0.04	0.04	0.03	0.04
Al^{iv}/Al^{vi}	8.50	8.00	8.00	4.20	6.25	8.50	4.75	5.50	6.33	5.75
Wo%	47.33	48.81	49.77	48.55	49.57	47.42	47.60	48.45	47.98	48.56
En%	39.36	39.12	36.26	40.15	38.65	39.56	40.25	40.81	40.44	39.43
Fs%	12.99	11.84	13.71	11.13	11.62	12.71	11.95	10.57	11.33	11.67

Structural formulae calculated on the basis of 6 oxygen anions and total iron expressed as Fe^{2+}. r: rim; c: core (of phenocrysts); m: microlite; mph: microphenocryst; Mg #: magnesium number; Wo: wollastonite; En: enstatite; Fs: ferrosilite. Mg # = $100Mg^{2+}/(Mg^{2+} + Fe^{2+})$.

Representative microprobe plagioclase compositions are presented in Table 4. Phenocryst cores have a narrow compositional range ($An_{73.7}Ab_{25.5}Or_{0.7}$–$An_{83.4}Ab_{16.3}Or_{0.3}$) while phenocryst rims show a wider compositional range ($An_{49.6}Ab_{41}Or_{9.3}$-$An_{73.7}Ab_{25.5}Or_{0.7}$) which overlaps with the microlite composition. Microphenocrysts have a similar composition to phenocryst cores (on average $An_{80.5}Ab_{19.0}Or_{0.5}$).

Representative microprobe analyses of titanomagnetite are presented in Table 5. FeO* (total iron) shows a narrow range (63.8–67.4 wt%) compared to the wider range shown by TiO_2 (14.3–21.3 wt%). The mineral is poor in MnO (0.44–0.71 wt%) and SiO_2 (0.04–0.24 wt%) with moderate amounts of Al_2O_3 (4.8–6.4 wt%) and MgO (4.8–6.7 wt%).

Whole rock geochemistry

Major and trace element concentrations were determined by X-ray fluorescence (XRF) spectrometry using a Philips PW 2404 automatic X-ray spectrometer at the Grant Institute of Earth Science, University of Edinburgh. The techniques used

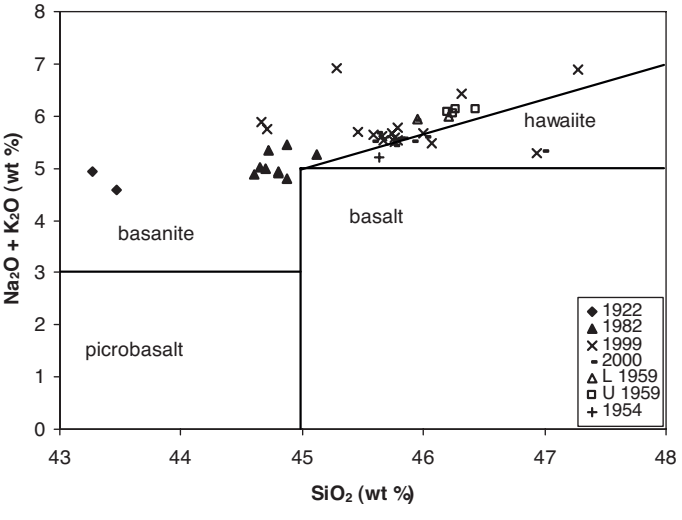

Fig. 5. The Total Alkali-Silica (TAS) diagram showing all Mt. Cameroon's 20th century lavas plotting as either basanite or hawaiite (after Le Bas et al. 1986. 'U' stands for upper site and 'L' for lower site).

Table 4. Representative electron microprobe analyses of plagioclase.

Sample C59LE (lower site)										
Analysis No.	1	2	3	4	5	6	7	8	9	10
Region	**m**	**mph**	**mph**	**r**	**r**	**r**	**c**	**c**	**c**	**c**
SiO_2	51.31	45.29	46.55	50.52	53.53	50.98	47.72	46.19	46.57	45.61
TiO_2	0.28	0.08	0.07	0.13	0.20	0.12	0.07	0.04	0.07	0.06
Al_2O_3	28.44	33.18	34.01	30.58	28.80	30.48	32.36	33.61	33.31	32.93
Cr_2O_3	0.00	0.01	0.01	0.02	0.04	0.02	0.02	0.00	0.00	0.00
FeO	1.02	0.58	0.59	0.65	0.64	0.69	0.56	0.55	0.57	0.55
NiO	0.02	0.03	0.00	0.04	0.00	0.01	0.00	0.04	0.00	0.01
MnO	0.00	0.02	0.00	0.00	0.00	0.01	0.01	0.00	0.02	0.00
MgO	0.13	0.06	0.07	0.09	0.07	0.10	0.05	0.04	0.05	0.06
CaO	11.26	16.88	16.77	13.62	11.09	13.18	15.67	16.80	16.73	17.00
Na_2O	4.54	2.21	2.18	4.38	5.70	4.45	3.00	2.30	2.30	2.19
K_2O	0.86	0.09	0.06	0.24	0.45	0.25	0.13	0.00	0.06	0.09
Total	97.85	98.44	100.31	100.26	100.52	100.29	99.59	99.56	99.68	98.50
Si^{4+}	2.37	2.13	2.14	2.31	2.42	2.33	2.21	2.14	2.15	2.14
Ti^{4+}	0.01	0.00	0.00	0.00	0.00	0.00	0.00	0.00	0.00	0.00
Al^{3+}	1.55	1.84	1.84	1.65	1.54	1.64	1.76	1.84	1.82	1.82
Cr^{3+}	0.00	0.00	0.00	0.00	0.00	0.00	0.00	0.00	0.00	0.00
Fe^{2+}	0.04	0.02	0.02	0.02	0.02	0.03	0.02	0.02	0.02	0.02
Ni^{2+}	0.00	0.00	0.00	0.00	0.00	0.00	0.00	0.00	0.00	0.00
Mn^{2+}	0.00	0.00	0.00	0.00	0.00	0.00	0.00	0.00	0.00	0.00
Mg^{2+}	0.01	0.00	0.00	0.01	0.01	0.01	0.00	0.00	0.00	0.00
Ca^{2+}	0.56	0.85	0.83	0.67	0.54	0.64	0.78	0.83	0.83	0.85
Na^{+}	0.41	0.20	0.19	0.39	0.50	0.39	0.27	0.21	0.21	0.20
K^{+}	0.05	0.01	0.00	0.01	0.03	0.01	0.01	0.00	0.00	0.01
Total	5.00	5.05	5.02	5.06	5.06	5.05	5.05	5.04	5.03	5.04
An%	54.92	80.41	80.64	62.37	50.54	61.23	73.73	80.17	79.79	80.65
Ab%	40.08	19.06	18.99	36.30	47.01	37.38	25.53	19.83	19.87	18.83
Or%	5.00	0.53	0.37	1.32	2.45	1.39	0.74	0.00	0.34	0.52

Structural formulae calculated on the basis of 8 oxygen anions and total iron expressed as Fe^{2+}. r: rim; c: core (of phenocrysts); mph: microphenocryst; m: microlite; An: anorthite; Ab: albite; Or: orthoclase. $An\% = 100Ca^{2+}/(Ca^{2+} + Na^{+} + K^{+})$.

Table 5. Representative electron microprobe analyses of titanomagnetite.

Sample C59LE (lower site)										
Analysis No.	1	2	3	4	5	6	7	8	9	10
Region	**mph**	**mph**	**r**	**r**	**r**	**c**	**c**	**c**	**c**	**c**
SiO_2	0.04	0.04	0.09	0.11	0.11	0.04	0.24	0.07	0.05	0.05
TiO_2	15.81	16.11	20.25	20.31	20.31	14.33	15.54	16.74	16.64	16.47
Al_2O_3	6.38	6.17	5.07	4.80	4.80	5.83	6.32	5.71	5.73	5.92
Cr_2O_3	0.08	0.08	0.14	0.14	0.14	0.13	0.20	0.32	0.32	1.10
FeO	67.32	67.35	65.47	65.40	65.40	67.23	63.78	67.05	66.82	66.43
NiO	0.09	0.09	0.09	0.04	0.04	0.06	0.05	0.00	0.02	0.04
MnO	0.48	0.44	0.71	0.70	0.70	0.56	0.47	0.53	0.56	0.52
MgO	6.37	6.48	4.99	4.83	4.83	6.61	6.67	6.60	6.56	6.70
CaO	0.00	0.00	0.09	0.08	0.08	0.02	0.18	0.00	0.01	0.00
Na_2O	0.00	0.00	0.07	0.09	0.09	0.07	0.00	0.07	0.00	0.00
Total	96.56	96.76	96.97	96.50	96.50	94.89	93.44	97.09	96.71	97.23
Si^{4+}	0.00	0.00	0.00	0.00	0.00	0.00	0.01	0.00	0.00	0.00
Ti^{4+}	0.47	0.48	0.59	0.60	0.60	0.44	0.47	0.49	0.49	0.48
Al^{3+}	0.30	0.29	0.23	0.22	0.22	0.28	0.30	0.26	0.27	0.27
Cr^{3+}	0.00	0.00	0.00	0.00	0.00	0.00	0.01	0.01	0.01	0.03
Fe^{2+}	2.22	2.21	2.13	2.14	2.14	2.28	2.15	2.19	2.20	2.16
Mn^{2+}	0.02	0.01	0.02	0.02	0.02	0.02	0.02	0.02	0.02	0.02
Mg^{2+}	0.37	0.38	0.29	0.28	0.28	0.40	0.40	0.38	0.38	0.39
Ca^{2+}	0.00	0.00	0.00	0.00	0.00	0.00	0.01	0.00	0.00	0.00
Na^{+}	0.00	0.00	0.01	0.01	0.01	0.01	0.00	0.01	0.00	0.00
Total	3.38	3.37	3.27	3.27	3.27	3.43	3.37	3.36	3.37	3.35

Structural formulae calculated on the basis of 4 oxygen anions and total Fe expressed as Fe^{2+}. r: rim; c: core; (of phenocrysts); mph: microphenocryst.

Table 6. Whole-rock XRF major and trace element compositions including CIPW norms of the 1959 Mt. Cameroon lavas together with data ranges for lavas from 1922 and 1982 (Fitton et al. 1983); 1999 and 2000 (Deruelle et al. 2000 and Suh et al. 2003) some of which were re-analysed at the same time with our samples. The 1954 data are from Suh et al. (2007).

Eruption Year	1959	1959	1959	1959	1959	1959	1959	1922	1954	1982	1999	2000
Sample No.	**C59LE**	**C59LF**	**C59U3**	**C59U5**	**C59U6**	**C59U7**	**C1**	**C25-C26**	**SI54/1**	**C192-C212**	**5-23/BA1-BA20**	**SM1-SM15**
Major Element concentrations expressed in weight percent												
SiO_2	45.95	46.21	46.43	46.27	46.24	46.20	46.22	43.27–43.47	45.63	44.61–45.12	44.66–47.28	45.59–46.99
TiO_2	3.22	3.25	3.18	3.16	3.20	3.22	3.15	3.08–3.39	3.12	3.38–3.44	2.98–3.20	3.10–3.18
Al_2O_3	15.71	15.76	15.99	15.86	15.84	15.88	16.04	12.05–13.14	15.01	14.99–15.46	14.78–16.87	14.93–15.59
Fe_2O_3	11.95	12.08	11.69	11.70	11.81	11.90	11.69	13.60–13.81	11.86	13.36–13.51	10.92–12.73	11.61–12.36
MnO	0.21	0.22	0.20	0.20	0.20	0.21	0.21	0.21–0.21	0.20	0.18–0.22	0.18–0.22	0.18–0.20
MgO	5.52	5.56	5.32	5.55	5.55	5.51	5.34	8.95–10.64	7.21	5.84–6.21	4.80–7.32	6.19–7.00
CaO	10.22	10.27	9.87	9.99	10.02	10.11	10.12	11.64–11.70	11.01	11.46–11.96	9.17–11.12	10.20–10.69
Na_2O	4.24	4.27	4.33	4.37	4.28	4.33	4.59	3.19–3.40	3.77	3.54–4.03	3.75–5.01	3.78–4.24
K_2O	1.71	1.73	1.81	1.77	1.76	1.75	1.77	1.40–1.54	1.45	1.27–1.43	1.54–2.00	1.52–1.66
P_2O_5	0.80	0.81	0.83	0.81	0.81	0.81	0.81	0.73–0.77	0.65	0.54–0.63	0.66–0.88	0.67–0.72
LOI	–0.39	–0.50	–0.40	–0.62	–0.40	–0.52	n.d.	n.d.	–0.34	n.d.	–0.60—0.07	–0.54—0.41
Total	99.14	99.65	99.25	99.06	99.32	99.40	99.93	100.00–100.17	99.57	100.09–100.84	99.55–99.92	99.58–99.99
Mg#	33.92	33.84	33.58	34.51	34.30	33.97	33.69	41.85–46.52	40.32	32.68–33.97	32.82–39.08	36.51–38.61
CIPW Norms expressed in weight percent												
Or	10.11	10.22	10.70	10.46	10.40	10.34	10.46	8.27–9.10	8.57	7.51–8.45	9.10–11.82	8.98–9.81
Ab	15.62	15.63	17.31	16.31	16.46	15.96	15.27	3.17–3.24	13.11	9.37–10.59	7.52–19.37	12.38–18.12
An	18.78	18.73	18.85	18.43	18.81	18.73	17.94	14.43–16.04	19.75	19.82–21.67	14.79–20.61	18.15–20.59
Ne	10.97	11.10	10.47	11.20	10.70	11.21	12.77	12.87–13.87	10.18	10.83–13.21	7.08–17.93	7.51–12.13
Di	22.09	22.29	20.44	21.36	21.18	21.63	22.33	30.29–31.42	25.06	26.63–28.83	17.84–27.84	22.52–24.92
Hy	0.00	0.00	0.00	0.00	0.00	0.00	0.00	0.00–0.00	0.00	0.00–0.00	0.00–0.00	0.00–0.00
Ol	12.26	12.38	12.22	12.35	12.50	12.35	11.62	17.49–20.27	13.58	12.28–12.80	11.58–15.34	12.88–14.79
Ilm	6.12	6.17	6.04	6.00	6.08	6.12	5.98	5.85–6.44	5.93	6.42–6.56	5.66–6.08	5.89–6.04
Mt	1.74	1.75	1.70	1.70	1.71	1.73	1.70	1.97–2.00	1.83	1.94–1.96	1.58–1.84	1.68–1.80
Ap	1.85	1.88	1.92	1.88	1.88	1.88	1.88	1.69–1.78	1.51	1.25–1.46	1.53–2.04	1.55–1.67
DI	36.70	36.95	38.48	37.97	37.56	37.51	38.50	24.38–26.14	31.86	28.30–31.25	32.44–43.07	33.03–35.79
Trace element concentrations expressed in ppm												
Rb	41.45	41.45	43.23	42.24	42.04	41.94	42.24	35.01–37.48	36.6	28.96–33.52	36.07–46.40	35.67–39.99
Ba	525.87	518.72	526.96	530.03	499.97	526.96	530.15	436.98–485.19	450	365.44–410.12	455.25–569.32	445.77–500.10
Nb	116.80	117.30	122.06	119.38	119.38	118.98	117.49	106.59–114.12	96.2	82.00–96.28	102.01–131.67	100.57–109.38
La	78.45	76.84	79.77	78.45	78.16	80.71	84.08	76.56–80.86	73.8	57.33–69.05	66.25–88.57	63.06–72.73
Ce	163.38	163.28	167.64	167.74	164.97	167.84	171.09	166.94–175.96	137.1	122.57–139.08	142.16–188.52	136.87–157.25
Sr	1131.60	1131.41	1150.17	1135.47	1124.63	1138.37	1148.14	1014.17–1108.48	1077	901.87–1023.75	992.12–1181.22	988.13–1060.83
Nd	74.14	74.14	73.05	74.34	73.65	74.24	74.23	72.38–76.92	59.2	55.14–64.59	62.77–80.53	60.48–69.39
Zn	107.51	105.59	105.68	106.78	107.51	107.78	107.07	118.73–123.10	113	116.65–127.79	99.66–119.46	99.77–110.23
Cu	65.24	62.21	66.05	59.49	52.32	63.42	67.90	68.86–81.73	76	104.59–111.93	55.36–78.75	66.75–76.52
Sc	14.80	15.90	14.00	15.20	15.20	15.20	14.35	27.80–31.21	26	20.57–27.80	11.34–23.44	19.28–23.87
Zr	393.07	395.99	409.23	402.13	402.90	400.67	399.98	352.38–370.10	339	300.39–337.39	351.11–425.98	349.34–373.78
Y	35.55	36.16	37.07	36.36	36.46	36.57	36.67	31.51–33.13	33.35	31.00–33.63	31.27–37.68	30.97–34.59
Ni	46.01	46.31	40.60	44.64	39.62	45.42	48.48	138.35–181.14	99	56.81–63.41	39.48–91.20	59.62–86.59
Cr	65.93	76.07	56.49	74.36	60.30	63.72	59.44	323.11–466.28	213	38.47–67.81	35.95–158.15	100.77–165.49
V	247.50	248.30	229.50	232.80	229.90	237.90	252.70	273.90–308.20	295	310.50–331.00	226.30–267.70	229.80–262.76

DI is differentiation index of Thornton and Tuttle (1960) defined as: DI = CIPW normative Qz + Or + Ab + Ne. Mg# (magnesium number) is 100MgO/(MgO+FeO), with FeO calculated as FeO = 0.9 Fe_2O_3* (total iron oxide), n.d.: not determined. 'U' samples are upper site while 'L' samples are lower site.

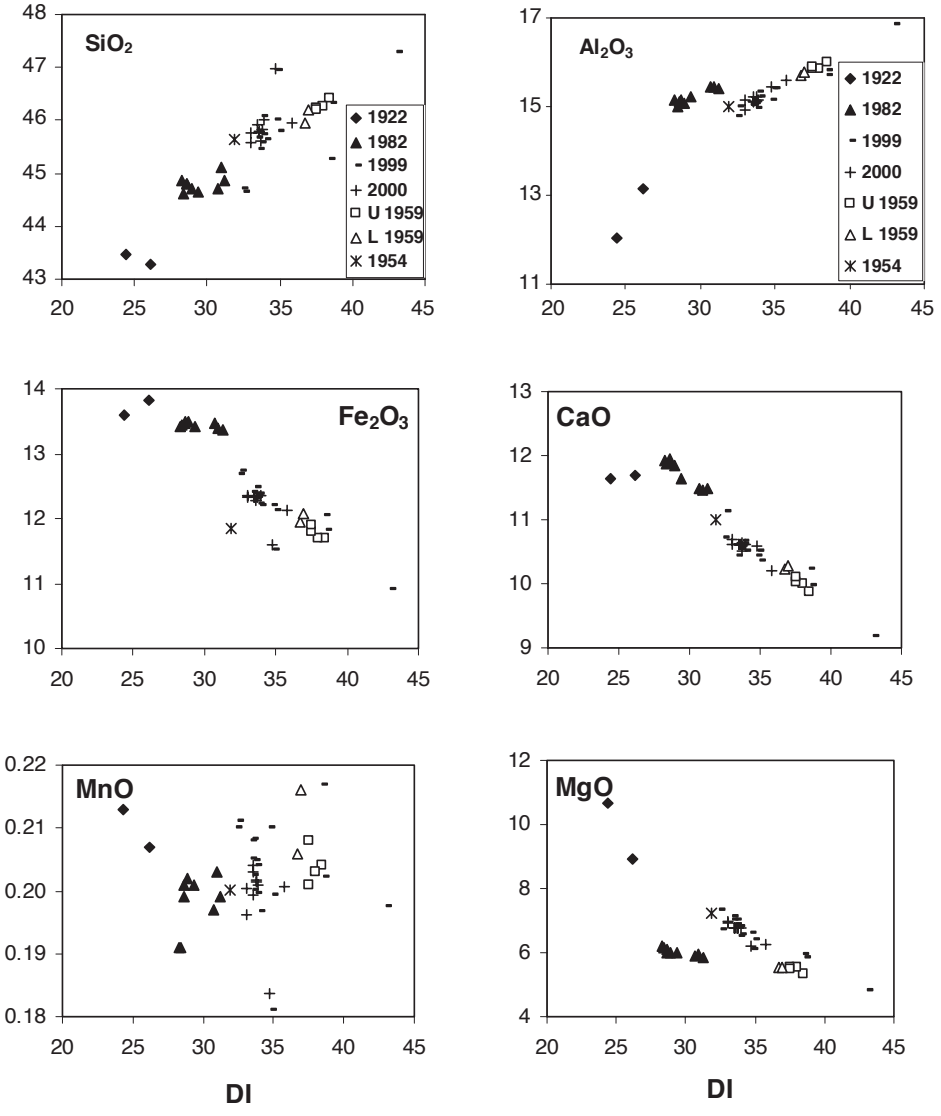

Fig. 6. Plot of major element oxides (wt%) versus DI for Mt. Cameroon's 20th century lavas (DI is differentiation index of Thornton and Tuttle (1960) defined as: DI = CIPW normative Qz + Or + Ab + Ne. 'U' stands for upper site and 'L' for lower site).

are essentially similar to those described by Fitton et al. (1998), with modifications noted by Fitton & Godard (2004). Analytical precision and accuracy are comparable to the values reported by Fitton et al. (1998).

The whole-rock compositions of the studied samples are presented in Table 6 alongside a reanalysis of the 1922, 1959 and 1982 samples of Fitton et al. (1983); the 1999 samples of Deruelle et al. (2000) and the 1999/2000 samples of Suh et al. (2003). The results of the reanalyzed samples remained the same within the precision limits. Also included is the 1954 sample of Suh et al. (2007).

On the TAS diagram (Fig. 5) the historical Mt. Cameroon lavas plot in two major fields – most within the basanite field with the 1954 and a few from the 1999/2000 upper site vents within the hawaiite field. All the samples contain normative nepheline (7.08–17.93).

Average silica content differs from flow to flow from 1922 (43.4 wt%), through 1982 (44.8 wt%), 1954 (45.63), 1999 (45.8 wt%), 2000 (45.9 wt%) to 1959 (46.2 wt%). Mg# {100MgO/(MgO+FeO), with FeO calculated as FeO = 0.9 Fe_2O_3* (total iron oxide)} shows the 1922 lava as the most primitive (Mg#: 44.2), followed by the 1954 (Mg#: 40.32), 2000 (Mg#: 37.8), 1999 (Mg#: 37.3), 1959 (Mg#: 34) and 1982 (Mg#: 33.2). The 1959 lavas are at the more evolved end of this spectrum. In addition, the 1959 lavas have the highest values of DI (37 on average), different from the 1999/2000 (34), 1954 (31.86), 1982 (28.6) and 1922 (25) (Table 6). The data also show that the upper site 1959 samples have average overall higher silica content (46.3wt%) and DI values (37.9) than the lower site samples (46.1 wt% and 36.8 respectively) (Table 6). SiO_2, Al_2O_3, P_2O_5, K_2O and Na_2O show a positive trend and MgO, CaO and Fe_2O_3* (total iron oxide) show a negative trend with DI (Fig. 6).

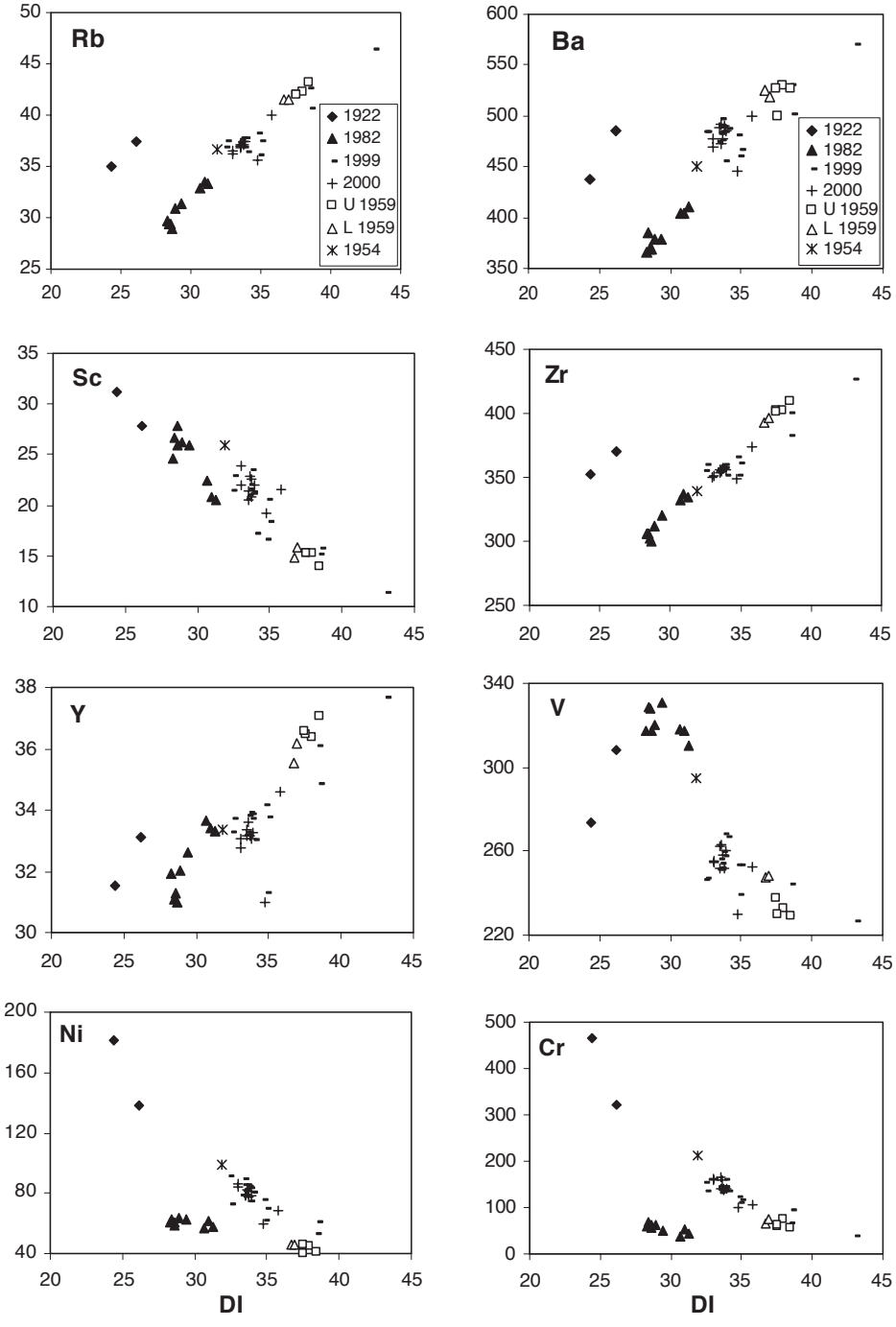

Fig. 7. Selected trace element variations (ppm) with DI for Mt. Cameroon's 20th century lavas (DI is differentiation index of Thornton and Tuttle (1960) defined as: DI = CIPW normative Qz + Or + Ab + Ne. 'U' stands for upper site and 'L' for lower site).

Figure 7 shows selected trace element variation diagrams with DI for the different lava flows. There is a negative correlation between the compatible elements (Cr, Ni, V and Sc) and DI. The 1959 lavas are poorer in Ni (<48.5 ppm) and Sc (<16 ppm) compared to others (>50 and >17 ppm respectively). Generally, the 1959 lavas have higher values for Nb, Y, Zr, Rb, Ba and Nd concentrations than those of other lavas (Table 6 and Fig. 7). The 1959 lower site lavas have lower Nb, Zr, Y, and Rb concentrations than the upper site lavas, attesting to the distinct characteristics of the two separate magmas erupted in 1959. On variation diagrams, all incompatible elements (Rb, Ba, Zr, Y, Nb, and Nd) show a positive correlation with DI (Fig. 7).

Discussion

The 1959 lava emplacement mechanism / eruption dynamics

We interpret the distinct layering shown by the upper site 1959 channels as indicative of decreasing lava level in the channels caused by diminishing extrusion rate with lava draining out of the channel. The layering indicates rapid changes in lava level in channels that represent fluctuations in lava supply. Vent size narrows towards the NW end, indicative of a linear migration of the fissure, which probably propagated in a zip-like manner from ESE–WNW. Suh et al. (2001) observed a SW–NE vent migration during the 1999 eruption and interpreted this as reflecting horizontal stress distribution. The vent alignment in 1959 indicates rotation of the stress field on the northeastern flanks of the volcano away from the dominant direction.

The fact that we have only a small spatter at the extreme WNW vent (Fig. 3a) shows that there was only little strombolian activity towards the end of the eruptive activity. At the ESE end of this spatter cone is a small bocca, supporting the idea that as degassing takes place at upper sites, the degassed magma drains out quietly at the lower sites. This relationship is also confirmed by the decrease in vesicle percentage and an increase in groundmass percentage away from the upper site vents (Table 1).

The very narrow and deep channels with less well developed levee structures that characterize the upper vent regions reflects high effusion rate, consistent with observations that flows classified as aa commonly result from relatively high effusion rate compared to pahoehoe lavas from the same magma type (Rowland & Walker 1990).

From our field observations and the studies of Suh et al. (2003) and Stansfield (2004), Mt. Cameroon flows commonly advance as aa but with proximal pahoehoe occurring locally near the vents or where lava tubes drain out and are examples of thermally immature lavas (Naranjo et al. 1992). This is consistent with observations of Soule et al. (2003), who pointed out that in Hawaii, flows that advanced as aa usually form pahoehoe surfaces near the vents, with the fraction of flow surface covered by pahoehoe decreasing systematically with distance from the vent. However, Soule et al. (2003) described the Hawaiian 1974 flows as having a proximal pahoehoe zone, a medial transition zone containing both pahoehoe and aa and a distal aa zone. This pattern is typical of Hawaiian lava flows (e.g. Lipman & Banks 1987; Wolfe et al. 1988), but differs from many Etnean flows which can be 100% aa at the vents (Soule et al. 2003), although Pinkerton and Sparks (1978) described flows at Etna that commenced as pahoehoe. At the proximal regions of the 1959 field, lava surfaces in the centre have experienced less cooling than at the channel margins and have experienced less shearing. As a consequence, the flow centre can remain as pahoehoe whereas the cooler and more sheared margins develop an aa clinker texture (Fig. 3b).

Magma origin / magmatic evolution

Primitive mantle normalized trace element spidergrams (Fig. 8a) show a similar pattern for all the Mt. Cameroon lavas with a relative depletion in K compared to similar incompatible elements such as Nb and La. A comparison between the spidergrams for Mt. Cameroon and both OIB and MORB from 45° N from the Mid-Atlantic Ridge, show a great similarity in pattern between Mt. Cameroon and OIB, indicating a similar mantle source. According to Dongmo et al. (2001), the mantle source is a pristine HIMU source due to the lack of relative enrichment in Rb, Ba, Th and K. In addition, incompatible elements plot on binary diagrams along straight lines (Fig. 8b) consistent with comagmatic relationships.

The difference in compatible and incompatible element ratios (e.g. V/Rb) for the 1959 lava and others, suggests that magma is supplied to the volcano in discrete batches from dif-

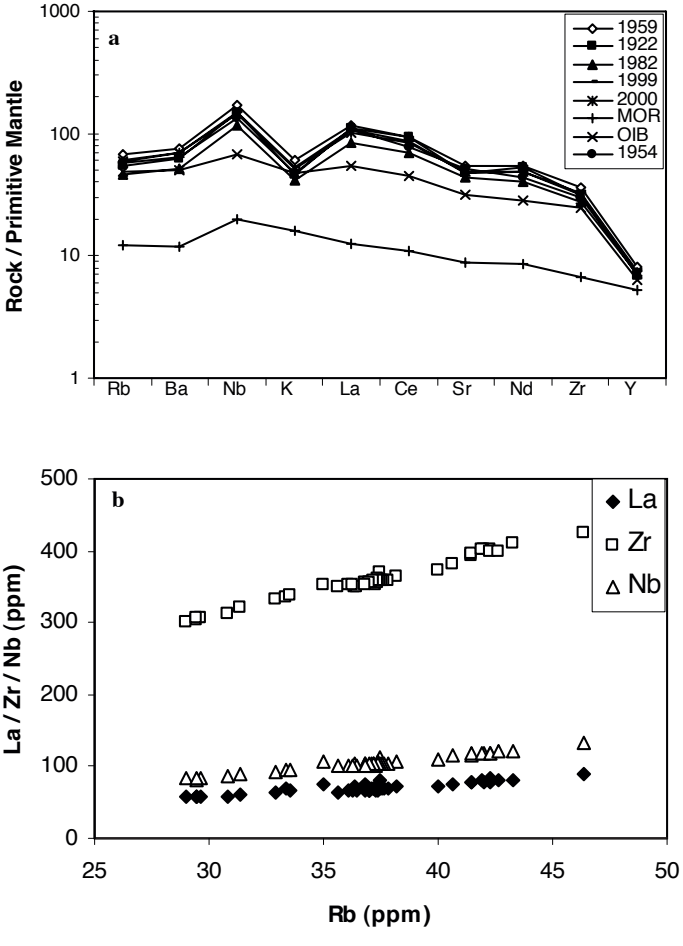

Fig. 8. a) Trace element patterns for Mount Cameroon lavas normalised to primitive mantle values of Sun and McDonough (1989) and compared to both OIB and MORB taken from 45° N in the Mid-Atlantic Ridge (values used for the plot are taken from Sun and McDonough 1989). b) Incompatible elements binary plots (La/Rb, Zr/Rb and Nb/Rb) show all 20th century Mt. Cameroon lavas plotting along straight lines, emphasizing their co-magmatic origin.

ferent chambers rather than from a single large evolving chamber as also suggested by Suh et al. (2003) for the 1982 and 1999 lavas and the lack of systematic evolution of the magmas with time from 1922 to 2000.

The 1959 and the 1999–2000 lavas (Suh et al., 2003) all show two types of clinopyroxenes. We interpret these as belonging to clinopyroxenes of origin 3 and 4 of Wass (1979). The isolated phenocrysts (discrete megacrysts) are interpreted to have formed at higher pressures, with resorption at the margins and at zone boundaries attributed to decompression. In contrast, the aggregate population that lacks resorption, sieve texture cores and overgrowths, indicates low pressure clinopyroxenes crystallization.

The 1959 upper site lavas show higher incompatible and lower compatible element contents than the lower site lavas and higher DI values, supporting their more evolved nature. In our interpretion, residual and more evolved fractionated magma (probably of the 1954 eruption) was pushed out first by gas pressure from degassing of a new batch of less evolved magma before the new batch of magma erupted at the lower site. The two contrasted magma batches did not mix and each maintained its geochemical identity. Fitton et al. (1983) also noticed such small but significant changes in composition for the 1982 eruption with the early more evolved lavas changing progressively to less evolved basic lavas.

Conclusion

Most Mount Cameroon eruptions exhibit activity at two sites, with the upper site vents being more explosive (producing cinder cones) while the lower sites remain quiet, spitting out large volumes of already degassed magma. Also, the available data shows that there is no progressive evolution of the magma with time since the 1959 lavas are more evolved. Morphological features displayed by lava flows vary according to proximity to the vents with lava tubes and inflation structures characterizing upper flow regions while pressure ridges and lava pinnacles characterize distal regions.

Acknowledgements

This work is part of a PhD thesis (by NMS) at the University of Buea undertaken under the sponsorship of the British Council Higher Education Link Project, "Understanding the Environment of Mount Cameroon" between the University of Buea and the University of Bristol. The authors remain grateful to the British Council for financial support to the analytical studies and stay of NMS in UK. RSJS acknowledges a Royal Society-Wolfson Merit Award. We thank Dr. Nick Odling (University of Edinburgh) for guiding and helping NMS with preparation of samples for XRF analysis and Ms. Gemma Stripp (University of Bristol) for guiding NMS with the microprobe analysis. Mr. C. Forba is thanked for tracing Figures 1 and 2. The quality of the paper was also greatly improved by the critical reviews of Andrea Marzoli, Jean Hernandez and Olivier Bachmann as well as the editorial comments of François Bussy.

REFERENCES

Ballentine, C.J., Lee, D.-C. & Halliday, A.N. 1997: Hafnium isotopic studies of the Cameroon line and new HIMU paradoxes. Chemical Geology 139, 111–124.

Deruelle, B., Bardintzeff, J-M., Cheminee, J-L., Ngounouno, I., Lissom, J., Nkoumbou, C., Etame, J., Hell, J-V., Tanyileke, G., N'ni, J., Ateba, B., Ntepe, N., Nono, A., Wandji, P., Fosso, J. & Nkouathio, D.G. 2000: Eruption simultanées de basalte alcalin et hawaiite au mont Cameroun (28 Mars–17 Avril 1999). Comptes Rendus de l'Académie de Sciences 331, 525–531.

Dongmo, A.K., Wandji, P., Pouclet, A., Vicat, J.P., Cheilletz, A., Nkouathio, D.G., Alexandrov, P. & Tchoua, F.M. 2001: Evolution volcanologique du mont Manengouba (Ligne du Cameroun); nouvelles données pétrographiques, géochimiques et géochronologiques. Comptes Rendus de l'Académie de Sciences 333, 155–162.

Fitton, J.G. 1980: The Benue trough and Cameroon Line – a migrating rift system in west Africa. Earth and Planetary Science Letters 51, 132–138.

Fitton, J.G. 1987: The Cameroon Line, West Africa: a comparison between oceanic and continental alkaline volcanism. In: Fitton, J.G. & Upton B.G.J (Eds.): Alkaline igneous rocks. Geological Society of London Special Publications 30, 273–291.

Fitton, J.G. & Dunlop, H. 1985: The Cameroon Line, West Africa, and its bearing on the origin of oceanic and continental alkali basalt. Earth and Planetary Science Letters 72, 23–38.

Fitton, J.G. & Godard, M. 2004: Origin and evolution of magmas on the Ontong Java Plateau. In: J.G. Fitton, J.J. Mahoney, P.J. Wallace & A.D. Saunders (Eds.): Origin and Evolution of the Ontong Java Plateau, Geological Society of London Special Publications 229, 151–178.

Fitton, J.G., Kilburn, C.R.J., Thirlwall, M.F. & Hughes, D.J. 1983: 1982 eruption of Mount Cameroon, West Africa. Nature 306, 327–332.

Fitton, J.G., Saunders, A.D., Larsen, L.M., Hardarson, B.S. & Norry, M.J. 1998: Volcanic rocks from the southeast Greenland margin at 63° N: composition, petrogenesis and mantle sources. Proceedings of the Ocean Drilling Program, Scientific Results 152, 331–350.

Geze, B. 1953: Les Volcans du Cameroun Occidental. Bulletin Volcanologique 13, 63–92.

Halliday, A.N., Dickin, A.P., Fallick, A.E. & Fitton, J.G. 1988: Mantle dynamics: a Nd, Sr, Pb and O isotopic study of the Cameroon Line volcanic chain. Journal of Petrology 29, 181–211.

Halliday, A.N., Davidson, J.P., Holden, P., DeWolf, C.P., Lee, D.-C. & Fitton, J.G. 1990: Trace element fractionation in plumes and the origin of HIMU mantle beneath the Cameroon Line. Nature 347, 523–528.

Jennings, J.H. 1959: The eruption of Mt. Cameroon, February–March 1959. Geography 44, 207–208.

Le Bas, M.J., Le Maitre, R.W., Streckeisen A. & Zanettin, B. 1986: Chemical classification of volcanic rocks based on the total alkali-silica diagram. Journal of Petrology 27, 745–750.

Lipman, P.W. & Banks, N.G. 1987: Aa flow dynamics, Mauna Loa 1984. In: Decker, R.W., Wright, T.L. & Stauffer, P.H (Eds.): Volcanism in Hawaii. US Geological Survey Professional Paper 1350, 1527–1567.

Marzoli, A., Renne, P.R., Piccirillo, E.M., Francesca, C., Bellieni, G., Melfi, A.J., Nyobe, J.B. & N'ni, J. 1999: Silicic magmas from the continental Cameroon Volcanic Line (Oku, Bambouto and Ngaoundere): $^{40}Ar/^{39}Ar$ dates, petrology, Sr-Nd-O isotopes and their petrogenetic significance. Contributions to Mineralogy and Petrology 135, 133–150.

Marzoli, A., Piccirillo, E.M., Renne, P.R., Bellieni, G., Iacumin, M., Nyobe, J.B. & Tongwa, A.T. 2000: The Cameroon Volcanic Line Revisited: Petrogenesis of Continental Basaltic Magmas from Lithospheric and Asthenospheric Mantle Sources. Journal of Petrology 41, 87–109.

Moreau, C., Regnoult, J.M., Deruelle, B. & Robineau, B. 1987: A new tectonic model for the Cameroon Line, Central Africa. Tectonophysics 139, 317–334.

Morimoto, N. 1989: Nomenclature of pyroxenes. Canadian Mineralogist 27, 143–156.

Naranjo, J.A., Sparks, R.S.J., Stasiuk, M., Moreno, H. & Ablay, G.J. 1992: Morphological, structural and textural variations in the 1988–1990 andesite lava of Lonquinmay Volcano, Chile. Geological Magazine 129, 657–678.

Njome, M.S., Suh, C.E. & Ghogomu, R.T. 2003: A microstructural approach to interpreting the structural setting of the Tombel graben, south western Cameroon. GeoActa 2, 181–200.

Pinkerton, H. & Sparks, R.S.J. 1978: Field measurements of the rheology of flowing lava. Nature 276, 383–385.

Rankenburg, K., Lassiter, J.C. & Brey, G. 2004: The role of continental crust and lithospheric mantle in the genesis of Cameroon Volcanic Line lavas: constraints from isotopic variations in lavas and megacrysts from the Biu and Jos plateaux. Journal of Petrology 46, 169–190.

Rowland, S.K. & Walker, G.P.L. 1990: Pahoehoe and aa in Hawaii: volumetric flow rate controls the lava structure. Bulletin of Volcanology 52, 631–641.

Soule, S.A., Cashman, K.V. & Kauahikaua, J.P. 2003: Examining flow emplacement through the surface morphology of three rapidly emplaced, solidified lava flows, Kilauea Volcano, Hawaii. Bulletin of Volcanology 66, 1–14.

Sparks, R.S.J., Pinkerton, H. & Hulme, G. 1976: Classification and formation of lava levees on Mount Etna, Sicily. Geology 4, 269–271.

Stansfield, A.S. 2004: Lava emplacement dynamics. Unpublished PhD Thesis, University of Bristol, Bristol, U.K., 291 pp.

Suh, C.E., Ayonghe, S.N. & Njumbe, E.S. 2001: Neotectonic earth movements related to the 1999 eruption of Cameroon Mountain, West Africa. Episodes 24, 9–12.

Suh, C.E., Sparks, R.S.J., Fitton, J.G., Ayonghe, S.N., Annen, C., Nana, R. & Luckman, A. 2003: The 1999 and 2000 eruptions of Mount Cameroon: eruption behaviour and petrochemistry of lava. Bulletin of Volcanology 65, 267–281.

Suh, C.E., Luhr, J.F. & Njome, M.S. 2007: Olivine-hosted glass inclusions in scoriae erupted in 1954–2000 at Mount Cameroon volcano, West Africa. Journal of Volcanology and Geothermal Research doi: 10.1016/j.jvolgeores.2007.07.004.

Sun, S-S. & McDonough, W.F. 1989: Chemical and isotopic systematics of oceanic basalts: implications for mantle composition and processes. In: Saunders, A.D. & Norry, M.L (Eds.): Magmatism in the ocean basins. Geological Society of London Special Publication 42, 313–345.

Thornton, E.P. & Tuttle, O.E. 1960: Chemistry of igneous rocks: Differentiation index. American Journal of Science 258, 664–684.

Ubangoh, R.U., Ateba, B., Ayonghe, S.N. & Ekodeck, G.E. 1997: Earthquake swarms of Mt. Cameroon, West Africa. Journal of African Earth Sciences 24, 413–424.

Ubangoh, R.U., Pacca, I.G. & Nyobe, J.B. 1998: Palaeomagnetism of the continental sector of the Cameroon Volcanic Line, West Africa. Geophysical Journal International 135, 362–374.

Wass, S.Y. 1979: Multiple origin of clinopyroxenes in alkali basaltic rocks. Lithos 12, 115–132.

Wolfe, E.W., Neal, C.A., Banks, N.G. & Duggan, T.J. 1988: Geological observations and chronology of eruptive events. In: Wolfe, E.W (Ed.): The Puu Oo eruption of Kilauea Volcano, Hawaii: episodes 1 through 20, January 3, 1983, through June 8, 1984. US Geological Survey Professional Paper 1463, 1–99.

Manuscript received March 26, 2007
Revision accepted October 18, 2007
Published Online first March 24, 2008
Edtitorial handling: François Bussy